Eur Biophys J (2010) 39:1503–1512
DOI 10.1007/s00249-010-0608-9

ORIGINAL PAPER

Dynamic correlation networks in human peroxisome proliferator-activated receptor-γ nuclear receptor protein

Jeremy Fidelak · Silvia Ferrer · Michael Oberlin · Dino Moras · Annick Dejaegere · Roland H. Stote

Received: 22 June 2009 / Revised: 9 April 2010 / Accepted: 21 April 2010 / Published online: 23 May 2010

Abstract Peroxisome proliferator-activated receptor-γ nuclear receptor (PPAR-γ) belongs to the superfamily of nuclear receptor proteins that function as ligand-dependent transcription factors and plays a specific physiological role as a regulator of lipid metabolism. A number of experimental studies have suggested that allostery plays an important role in the functioning of PPAR-γ. Here we use normal-mode analysis of PPAR-γ to characterize a network of dynamically coupled amino acids that link physiologically relevant binding surfaces such as the ligand-dependent activation domain AF-2 with the ligand binding site and the heterodimer interface. Multiple calculations were done in both the presence and absence of the agonist rosiglitazone, and the differences in dynamics were characterized. The global dynamics of the ligand binding domain were affected by the ligand, and in particular, changes to the network of dynamically correlated amino acids were observed with only small changes in conformation. These results suggest that changes in dynamic couplings can be functionally significant with respect to the transmission of allosteric signals.

Keywords Molecular dynamics · Nuclear receptor · Allostery · Normal mode · Protein

J. Fidelak and S. Ferrer contributed equally to this work.

J. Fidelak · S. Ferrer · M. Oberlin · D. Moras · A. Dejaegere (✉) · R. H. Stote (✉)
Structural Biology and Genomics Department, Institut de Génétique et de Biologie Moléculaire et Cellulaire, BP 10413, Illkirch, Strasbourg, France
e-mail: annick@igbmc.fr

R. H. Stote
e-mail: rstote@igbmc.fr

Introduction

Peroxisome proliferator-activated receptor gamma (PPAR-γ) belongs to the superfamily of nuclear receptors (NRs) that are ligand-dependent transcription factors (Mangelsdorf et al. 1995). The nuclear receptors PPAR-α, PPAR-β/δ, and PPAR-γ are important regulators of lipid storage and metabolism (Ferre 2004) and have been implicated in diseases associated with dysregulation of lipid levels, such as obesity, cardiovascular disease, and type 2 diabetes. As a class II ligand-activated nuclear hormone receptor (Brelivet et al. 2004), PPAR-γ forms heterodimers with the retinoid X receptor (RXR) (Gampe et al. 2000) and binds to the peroxisome proliferator response elements in the target gene, thus regulating the transcription of specific genes. Natural ligands of PPAR-γ include long-chain polyunsaturated fatty acids and natural prostaglandins (Kliewer et al. 1997). The importance of PPAR-γ as a medicinal target became clear when it was identified as the cognate receptor for the thiazolidinedione (TZD) class of insulin-sensitizing drugs (Lehmann et al. 1995), and synthetic PPAR-γ ligands, such as rosiglitazone and pioglitazone, have found important use in antidiabetic treatments. New synthetic ligands of PPAR-γ are sought as novel therapeutic compounds for a number of human diseases, including type II diabetes (Lehmann et al. 1995) and atherosclerosis (Verma and Szmitko 2006), and for the treatment of inflammation (Kostadinova et al. 2005).

Three-dimensional structures of the ligand binding domain (LBD) of PPAR-γ in the presence of different ligands have been solved by X-ray crystallography (Gampe et al. 2000; Bruning et al. 2007; Cronet et al. 2001; Nolte et al. 1998; Ostberg et al. 2004; Ebdrup et al. 2003; Sauerberg et al. 2002; Uppenberg et al. 1998; Li et al. 2005; Xu et al. 2001; Montanari et al. 2008). The structure of the

folded regions of the PPAR-γ/RXR-α heterodimer on DNA was recently determined (Chandra et al. 2008). Structures of the ligand-bound LBD of PPAR-γ display the general fold of the NR superfamily (Renaud and Moras 2000), which consists of a three-layer antiparallel α-helical sandwich. The carboxy-terminal helix, H12, is found to fold against the LBD to form an interaction surface for transcriptional coactivators. In spite of the fact that its global topology is similar to those of other nuclear receptors, structural analysis has shown that PPAR-γ has a short helix positioned between H2 and H3, referred to as H2′, that is generally absent in other receptors.

Structural dynamics and stabilization of H12 are recognized as important components of nuclear receptor function (Nettles et al. 2004; Nagy and Schwabe 2004), and significant efforts have been made toward elucidating their roles in the activation of PPAR-γ. While much of this effort has focused on structural properties of H12, primarily by X-ray crystallography, dynamical properties have also been probed. Fluorescence studies by Kallenberger et al. (2003) showed that, for full PPAR-γ agonists, the degree of agonism was proportional to the degree of H12 stabilization induced by binding. Amide hydrogen/deuterium exchange (H/D-Ex) was used to study the PPAR-γ LBD in the presence and absence of two full agonists, a partial agonist (nTZDpa), and a covalent antagonist (GW9662) (Hamuro et al. 2006). The results showed that the full agonists altered the H/D-Ex rates to a greater extent than did the partial agonist or the antagonist and, in particular, led to stabilization of H12. Neither the partial agonist nor the antagonist perturbed the H/D-Ex rates in this region on the time scale probed. A more recent amide H/D-Ex kinetics study of six PPAR-γ complexes with full and partial agonists revealed that each ligand induced unique changes to the dynamics of the LBD (Bruning et al. 2007). Consistent with the earlier study, full agonists were shown to stabilize H12, whereas intermediate and partial agonists did not. In the case of the latter, differential stabilization of other regions of the binding pocket was observed, in particular the β-sheet region. In this experiment, the ligand-dependent transcriptional activity of PPAR-γ could not be rationalized solely through changes to the dynamics of H12, and other regions of the protein were implicated. Given the structural similarity of full and partial agonist-bound complexes of PPAR-γ, it is reasonable to suggest that agonism depends not only on the H12 conformation, but on the dynamics, in particular of H12, but more generally of the entire ligand binding domain. In this view, protein fluctuations and their changes resulting from ligand binding play an important role. A similar idea was proposed as a general mechanism for allostery (Cooper and Dryden 1984), where changes in protein fluctuations result in changes in binding entropy. Numerous examples have since been discussed in the literature (Tsai et al. 2008).

In this work, we used normal-mode analysis to characterize the detailed changes to protein fluctuations as a function of ligand binding. Normal-mode analysis permits the simulation of the collective, low-frequency dynamics of the PPAR-γ LBD. Calculations were done for both the apo- and holo-PPAR-γ LBD/rosiglitazone complex. The principal result of the present work is the identification of a network of dynamically coupled amino acids in the ligand binding domain of PPAR-γ. This long-range dynamic network was identified by the calculation of equal-time cross-correlation maps using the low-frequency vibrational modes obtained from the normal-mode analysis. This network dynamically couples different physiologically relevant regions of the LBD and is also responsible for the transmission of information related to ligand binding. In particular, our results show that the stabilization induced by binding of the full agonist rosiglitazone, as characterized by H/D exchange analysis of Bruning et al. (2007), follows the pattern of changes observed to the correlation network upon ligand removal. These results provide a more detailed view of the dynamics of PPAR-γ than that obtained from analysis of crystallographic temperature factors or by root-mean-square (RMS) fluctuations calculated by molecular dynamics simulations. The current study provides new insights into the role and effects of ligand binding.

Results

The published crystal structure of PPAR-γ in complex with the full agonist rosiglitazone and a peptide from the coactivator SRC-1 was used as the initial structure for this normal-mode study (Nolte et al. 1998). A schematic drawing of PPAR-γ in complex with rosiglitazone and the coactivator peptide, with the secondary structure labeled, is shown in Fig. 1. Normal-mode analyses were done on a total of 20 energy-minimized structures: 10 in the presence and 10 in the absence of the agonist. The energy-minimization protocol was slightly modified for each structure by randomly changing the number of initial minimization steps, thus generating an ensemble of structures in the vicinity of the crystal structure. The SRC-1 coactivator peptide was included in all calculations. Although the apo-structure bound to a coactivator is not necessarily the functional physiological state of the protein, this fictive reference state gave us a means to assess the effects of the ligand without needing to consider large-scale conformational changes of the LDB, which evidently occur in the absence of ligand. The results from the analysis were averaged over each binding state in order to remove any

dependencies that may arise from a single-structure normal-mode calculation.

Energy minimization and normal-mode analysis

The root-mean-square deviations (RMSD) of the PPAR-γ LBD with respect to the initial experimental structure ranged from 1.0 to 1.4 Å for the ten apo- and ten holo-structures. The backbone RMSD between each individual energy-minimized structure within a group and the other structures within the same group did not exceed 0.6 Å, thus indicating that the energy-minimized structures were slightly different yet distributed around a common experimental structure. In general, the largest differences in structure were localized to the loops that connect helices H2/H2′ and helices H2′/H3. Some structural changes occurred in the H11/H12 loop, as well as in the C-terminal end of helix H12 and the C-terminal end of the coactivator peptide. All major structural elements were, however, accurately represented after energy minimization. These structures were then used for the normal-mode calculations. For all structures, the six lowest frequencies, which correspond to translational and rotational degrees of freedom, were essentially zero; all other frequencies were positive.

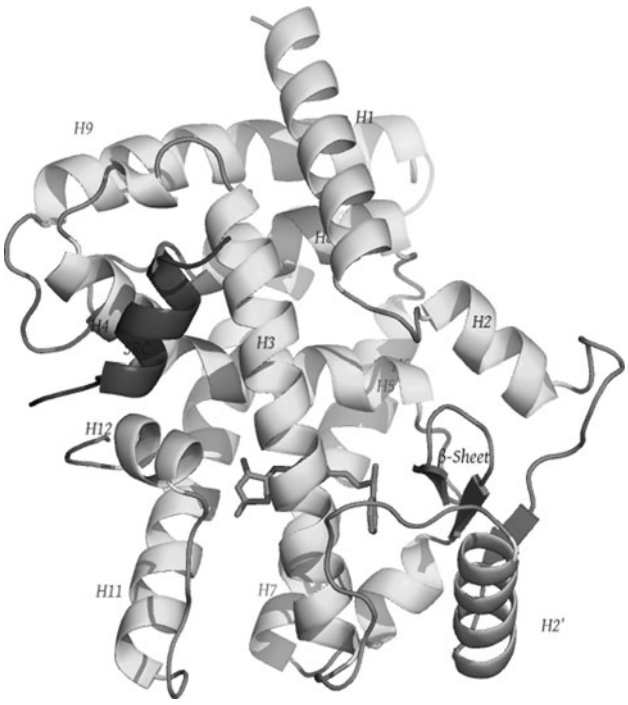

Fig. 1 Cartoon of PPAR-γ with labeling of helices. The ligand rosiglitazone is shown in *stick format*, and the SRC-1 coactivator peptide is shown in *dark gray*

Intrinsic dynamics of PPAR-γ

The atomic root-mean-square fluctuations (RMSF) were calculated from the normal modes for the two sets of ten energy-minimized structures (apo and holo) using

$$\left\langle (\Delta r_i)^2 \right\rangle = k_B T \sum_{k=7}^{3N} y_{i,k}^2 \Big/ (M_i \omega_k^2), \quad (1)$$

where $\langle (\Delta r_i)^2 \rangle$ is the time-averaged mean square displacement of atom i, ω_k is the frequency of mode k, $y_{i,k}$ is the displacement of atom i under mode k, N is the number of atoms, and M_i is the mass of atom i (Brooks et al. 1995; Marques and Sanejouand 1995). The results were averaged by residue for the holo complex and compared with the fluctuations calculated from the crystallographic B-factors (Fig. 2). A similar RMSF pattern was obtained, although the calculated fluctuations tended to be lower in absolute value than the experimental ones. This has been observed in other calculations and is due, in part, to the crystal lattice disorder contribution to the B-factors (Frauenfelder et al. 1979). From the RMSFs, we find that all the loop regions (for example, loops between H2/H2′, H2′/H3, H9/H10, and H11/H12), as well as the N- and C-terminals of the protein and the coactivator peptide, display the highest flexibility. While this general dynamical behavior has been well established from the temperature factors available from the numerous crystallographic structures found in the Protein Data Bank (Berman et al. 2000; Bernstein et al. 1977), this favorable comparison between theoretical and experimental values establishes that our calculations provide a good representation of the molecular-level dynamics, thus setting the stage for subsequent analysis.

Correlated motion analysis shows coupling between distant regions of the LBD

From the first 3,000 low-frequency vibrational modes and frequencies, the covariance matrix of spatial atomic displacements was calculated for each PPAR-γ energy-minimized structure using

$$\left\langle \Delta r_i \Delta r_j \right\rangle = k_B T \sum_{k=7}^{3N} (y_{i,k} y_{j,k}) \Big/ (M_i^{1/2} M_j^{1/2} \omega_k^2), \quad (2)$$

where $\langle \Delta r_i \Delta r_j \rangle$ is the time-averaged correlated displacement of atoms i and j, ω_k is the frequency of mode k, $y_{i,k}$ is the displacement of atom i under mode k, N is the number of atoms, and M_i is the mass of atom i (Brooks et al. 1995; Marques and Sanejouand 1995). The correlation values were normalized by the geometric mean of the fluctuation values for the individual degrees of freedom. These results provide a measure of correlated internal motions. The results are presented in the form of correlation maps, where

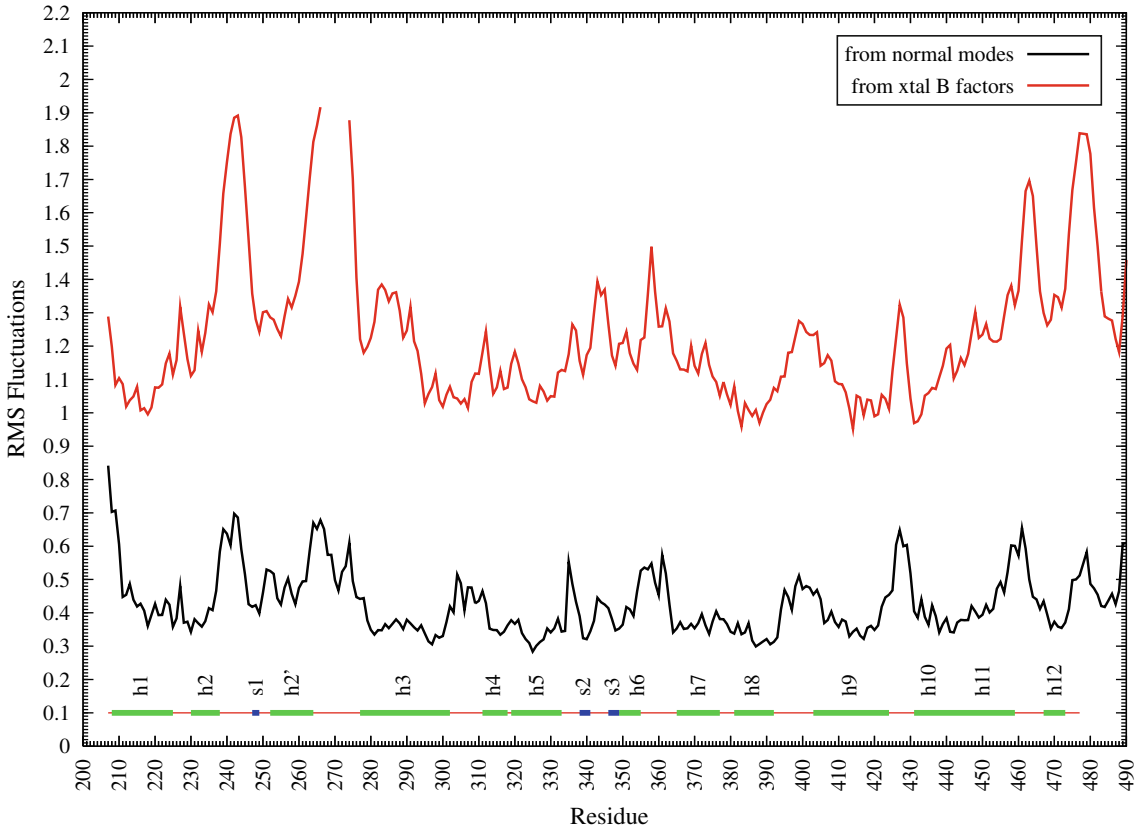

Fig. 2 Atomic fluctuations in Å calculated from the normal modes and experimental *B*-factors. The normal-mode fluctuations are averaged over ten holo structures

the standard convention was used with a positive value between 0 and 1 reflecting correlated motion and a negative coefficient between 0 and −1 reflecting anticorrelated motion. In perfectly correlated motion, both atoms move in phase, while in perfectly anticorrelated motion the atoms move in antiphase.

The correlation map for PPAR-γ complexed with the ligand and coactivator peptide is shown in Fig. 3. As for the RMSD calculations of Section "Energy minimization and normal-mode analysis", the results presented here are averaged over the ten structures obtained from the energy-minimization protocol. The variance of the correlation coefficients was on the order of 0.001, thus demonstrating convergence of the results. General structural elements of PPAR-γ can be identified by the pattern of cross-correlations. The enlargements along the diagonal are typical for α-helices, where motions of amino acids adjacent in sequence are correlated. Typically, in a nonstructured region such as the loop between H2 and H2′, the strong correlations (e.g., $\geq$0.4 in a normal-mode calculation) for a residue i will extend between $i-3$ and $i+3$. One can expect that residues very near in sequence will move in a correlated fashion; however, in a helix, strong correlations extend on a much longer range, from i to $i \pm (6–8)$. For long α-helices, strong correlations may not extend along the entire length, so helices cannot necessarily be viewed strictly as rigid structural elements. Cross-correlations that extend as plumes from the diagonal correspond to anti-parallel elements of secondary structure. Although, they are usually observed for antiparallel β-sheets, in the case of the LBD fold, which is mostly helical, they correspond to helices that are packed against each other in an antiparallel fashion. Correlated motions between secondary structural elements that are not adjacent in sequence are indicative of spatial proximity in the three-dimensional (3D) structure in a number of cases. This gives rise to islands of correlated and uncorrelated motions (Fig. 3).

For PPAR-γ, cross-correlations are found between multiple structural elements, some of which result from specific contacts, while others are longer range in nature. For example, cross-correlations between H1 and H9 result from hydrophobic contacts between Leu211 and Leu214 of H1 with H9. H1 is further correlated with H8 and H3 and shows anticorrelation with H12. There are long-range cross-correlations between H1 and H2′ and between H1 and H10/H11. These correlated motions do not result from direct van der Waals contact and thus dynamically join two distant, but physiologically important, elements of

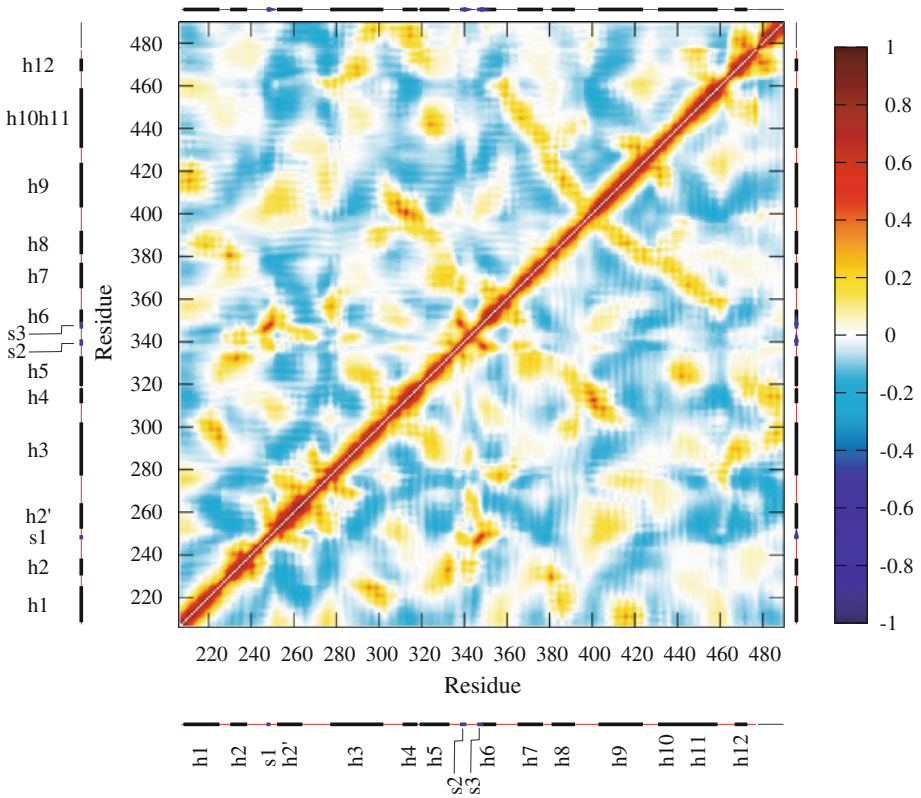

Fig. 3 Average correlation map calculated from normal modes for PPAR-γ complexed to rosiglitazone and the coactivator peptide SRC-1

PPAR-γ. Long-range cross-correlations are also observed between H1/loop H1–H2 and H6/H7, as well as between H2′ and loop H8-H9 and H9. H3 is a long helix (25 residues), and the analysis shows that the motions of its N- and C-terminal ends are correlated with different structural elements. For example, the H3 C-terminal end, beginning from Val293 shows significant correlation with H1, while the H3 N-terminal end does not. Between H3 and H5, there are correlations due to the presence of a hydrophobic cluster made up from Val293 (H3), Val322 (H5), and Ile326 (H5). The C-terminal end of H3 also displays some correlated motion with H8. The N-terminal end of H3 is less correlated with H8 but shows correlation with the loop H11–H12, as well as with H12. These results suggest that the dynamics of the N- and C-terminal ends of H3 can be considered somewhat independently. The motion of H4/H5 shows a significant number of cross-correlations with all other helices in the protein, which reflects their central positions in the protein structure. The motions of these helices are anticorrelated with respect to H9. And, in addition to its correlation with H4/H5, the motions of H6 and H7 are correlated with H10/H11. Cross-correlations between the different layers of the LBD α-sandwich are observed in the form of long plumes in the maps. In Fig. 3, cross-correlations of the region between H1 and H3 (one side of the sandwich) with H4/H5, H8, and the middle of H9 can be seen. Long-range correlations across the sandwich structure are also observed, in particular between H1 and H10/H11.

Helices H10/H11 are key components of the interface formed with RXR under physiological conditions. These helices are significantly correlated to helices H4/H5, H7, and H8 and anticorrelated to H9. At the C-terminal end, there are strong correlations between all structural elements in the region encompassing H11, loop 11–12, and H12. H12 is cross-correlated with H3, H4/H5, and H10/H11. Also observable are strong correlations of the β-sheet region and H6 and H7. Significant anticorrelation is observed between the β-sheet region and H10/H11, as well as with H9.

Effect of ligand removal on correlated motions

To assess the impact of ligand binding on the dynamics of the PPAR-γ LBD, we compared the cross-correlations calculated for the full complex (protein + ligand + coactivator peptide) with the correlations calculated for the complex in the absence of the ligand but in the presence of the coactivator peptide. The absolute difference in cross-correlations was calculated for each amino acid pair between the holo- and apo-states and averaged over the ten structures. We define the by-residue ligand impact factor (LIF), which is, for amino acid i, the normalized sum of the absolute differences in pair

correlations between amino acid i and all amino acids $j \neq i$, given by

$$a_i = \frac{1}{a_{\max}} \sum_{\substack{j=1 \\ j \neq i}}^{N_{\text{res}}} \left| c_{ij}^{\text{holo}} - c_{ij}^{\text{apo}} \right|, \quad (3)$$

where c_{ij}^{X} is the cross-correlation for the residue pair ij, and X refers to the holo or apo forms; N_{res} is the total number of residues. The quantity a_i serves as a measure of the effect of ligand binding on the correlated dynamics of residue i. The maximum value of a_i is $a_{\max}$ and therefore serves as a normalization coefficient. If there is little change to the cross-correlation coefficients for residue i, then the value will be near 0. If the residue is strongly affected by ligand binding, the value will approach 1. The a_i values were color-coded and superposed onto the structure of PPAR-γ; see Fig. 4a, which projects the LIF onto the 3D structure of PPAR-γ. The colors range from blue to red, where blue corresponds to amino acids that show little change in cross-correlation upon ligand removal, to red, which signifies amino acids that show significant changes to their correlations. We see that ligand binding influences the global motions of PPAR-γ as there are few regions that show no change in the cross-correlations. Two principal regions show significant changes in cross-correlations upon ligand removal. These include the mid-region of H3, and the C-terminal end of H12, where direct interactions with the ligand occur. Ligand removal also influences the coupling of H12 to H10/H11 as well as coupling of the β-sheet regions to other parts of the protein. Couplings of the β-sheet region affected by ligand binding are with structural elements surrounding the ligand binding pocket, as well as with H12. H/D exchange studies implicated the β-sheet region of the LDB as being affected by ligand binding. Couplings involving the dimer interface are also influenced by ligand binding.

The changes to the atomic fluctuations calculated from the normal modes, as well as the changes to the H/D exchange rates taken from the work of Bruning et al. (2007), were similarly projected onto the 3D structure of PPAR-γ, see Fig. 4b and c, respectively. The changes in atomic flexibility are less extensive than the changes in correlated motions. Changes in H/D exchange rates show a similar pattern to the changes in correlation coefficients.

Ligand binding exerts an influence on the dynamics in and generally around the ligand binding pocket. These results are consistent with nuclear magnetic resonance (NMR) studies of apo and holo PPAR-γ and PPAR-α, which showed that the lower portion of the ligand-free LBD shows exchange broadening on a millisecond timescale (Cronet et al. 2001; Johnson et al. 2000). This suggested that there is significant conformational mobility and that the lower portion of the receptor is rather

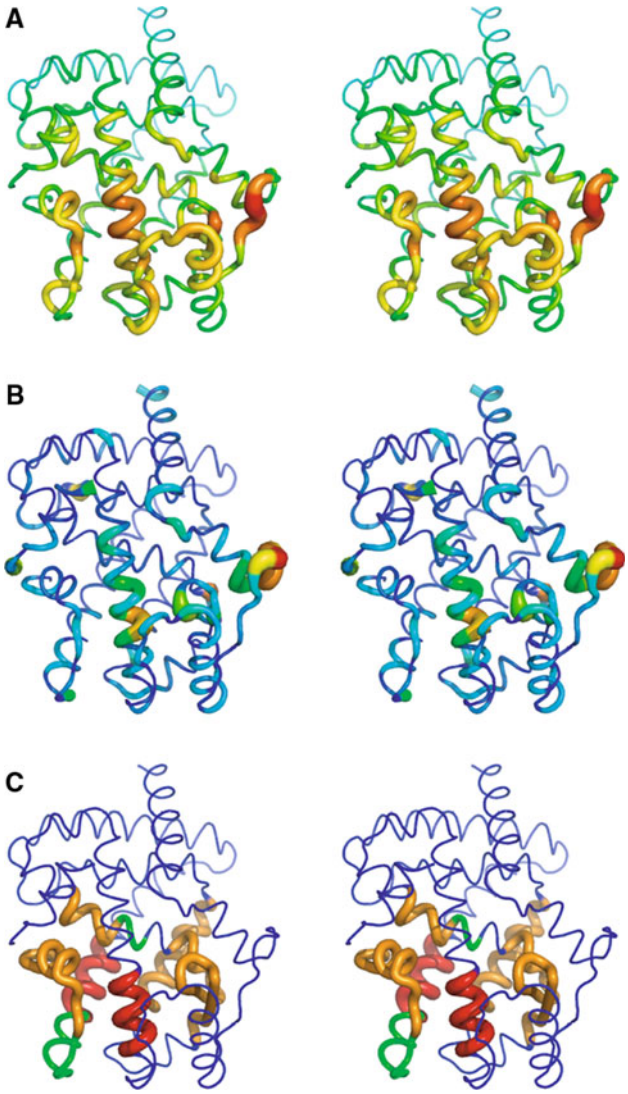

Fig. 4 Normalized differences mapped onto the three-dimensional structure of PPAR-γ displayed in cross-eyed stereo: **a** correlation coefficients, **b** atomic fluctuations, and **c** H/D exchange rates. The differences are between the protein complex in the presence and absence of rosiglitazone, and the color scales are from *blue* ($a_i = 0$) to *red* ($a_i = 1$), where i is the ith amino acid. Rosiglitazone is shown in *green* for purpose of orientation

dynamic (Gee and Katzenellenbogen 2001). The present results show that significant changes in dynamics due to ligand removal, as measured by the cross-correlations, are distributed over the lower portion of the protein. The computational results are also coherent with the observed changes in H/D exchange rates for the different regions of PPAR-γ (Bruning et al. 2007). The crystallographic studies of these protein complexes showed no significant change in structure (Bruning et al. 2007). The study identified the N-terminal region of H3, the β-sheet regions, a mid-segment of H10/H11, and H12 as regions that undergo the most significant changes in H/D exchange rate upon binding of rosiglitazone. We superposed the sequence-dependent change

in H/D exchange rates onto the 3D structure of PPAR-γ (Fig. 4c). The color gradient, from blue to red, as well as the increasing thickness of the coil, reflects a decreasing rate of exchange as a result of rosiglitazone. When comparing this figure with protein–ligand contacts determined based on atom–atom distance of 5 Å or less, one sees that, in some instances, changes in H/D exchange rates extend beyond ligand contacts, for example, along H7, where there is only one point of contact between the ligand and the protein. However, H7 exhibits significant changes in H/D exchange rates, as measured by the experiments of Bruning et al. (2007). From the mapping of the changes in correlated motions, we see a similar pattern along H7, although with a smaller magnitude, but more coherent with the H/D exchange data than the change in RMS fluctuations (Fig. 4b), where the propagation is much less extensive. Qualitatively, we see better coherence between the changes in H/D exchange rate and changes in correlation than with changes in anisotropic fluctuations. Interestingly, these longer-range changes in H/D exchange patterns follow the changes in the correlation coefficients, as shown in Fig. 4a, an exception being the loop region between H1 and H3, where longer-range correlation changes are observed, but no significant changes in H/D exchange rates are observed. A probable reason is that this region remains quite dynamic in the presence of the ligand and therefore always experiences exchange on the time scale of the experiments. This does not preclude the fact that faster dynamics, as would be probed by the normal-mode calculations, could be affected by ligand binding.

Discussion

In this work, we identified a network of dynamically linked amino acids in the ligand binding domain of PPAR-γ using normal-mode analysis. This network arises primarily from the low-frequency collective motions, which have been implicated in biological function for many other proteins. This is the first such characterization of a nuclear receptor protein by this method and, when combined with results from experimental studies such as x-ray diffraction for structural studies and H/D exchange studies, a more comprehensive picture of the global dynamical motions of the PPAR-γ LBD emerges.

Analysis of the correlated motions indicated that the presence of the ligand influences the low-frequency modes and affects the dynamics not only in and around the ligand binding pocket but also for more distant amino acids, including those at the dimer interface. These local conformational fluctuations couple different protein binding interfaces, and changes in these couplings induced by ligand binding may constitute a fundamental contribution to agonism in nuclear receptor proteins. Numerous mutations of PPAR-γ have been either identified or engineered, and their effects have been described in the literature (Agarwal and Garg 2002; Hasstedt et al. 2001; Hegele et al. 2002; Ludtke et al. 2007). While many of these mutations have been explicitly engineered to better elucidate binding studies, several have been associated with a number of human diseases. In particular, the mutations V290M(H3) and P467L(H12) have been associated with diseases such as insulin resistance, hypertension, hypertriglyceridemia, and early-onset diabetes (Hasstedt et al. 2001). Familial partial lipodystrophy, characterized by altered distribution of subcutaneous fat, muscular hypertrophy, and symptoms of metabolic syndrome, has been associated with several mutations in the PPAR-γ gene. These include F360L(H6) (Hegele et al. 2002), and the amino acids of loop 8–9, D396N (Ludtke et al. 2007), and R397C (Agarwal and Garg 2002). Interestingly, we found that all these mutations fall into regions of highly correlated motions that couple different binding surfaces of the LBD. Located in H3, the motions of V290 are strongly coupled to the motions of H1, H5, and H12, which are themselves strongly coupled to other helices of the LBD. P467 is located in the N-terminal part of H12 and is found in islands of strong coupling to H3 and H11. F360 is in loop 6–7, which shows significant coupling to H11 and also to the N-terminal end of H3. D396 and R397 are both located in loop H8–H9 and are found in an island of correlated motions with the central helix H4/5. The mutation Y473A in H12 was shown to disrupt full agonist binding and activation but not partial agonist (Einstein et al. 2008). This residue is found in an island of correlation that couples H12 with H3, H4/H5, and H10/H11. Interestingly, these mutations all fall into regions of elevated changes in correlation upon ligand removal (high LIFs), suggesting that changes to amino acids in these regions are more likely to affect protein function than are changes to amino acids in region of low correlation change.

In the experimental work of Bruning et al. (2007), amide H/D exchange kinetics were determined for PPAR-γ as a function of ligand, where the ligand ranged from full to partial agonists, and they characterized the changes in H/D exchange rates for different regions of the PPAR-γ ligand binding domain. The changes ranged from no effect to up to a decrease by 26% in the rate of exchange. We compared these differences in exchange rates to both changes in atomic fluctuations upon ligand removal as well as to changes in amino acid correlations. As shown in Fig. 4, those regions of the protein that exhibited the largest changes in H/D exchange rate correspond to those regions that showed the largest change in atomic fluctuations and correlations upon removal of the ligand.

The question of agonism, both full and partial, in nuclear receptor proteins remains a subject of significant interest, and much remains to be understood, particularly at the structural level. In this study, we showed, from a dynamics point of view, that there exists a network derived from the low-frequency collective motions that couples different physiologically important interfaces of the ligand binding domain and that this network can be influenced by ligand binding. A challenge that remains is to determine to what degree perturbing this network may contribute to full or partial agonism of nuclear receptor function. In the continuation of this work, then, we will use the large number of structures of PPAR-γ complexed to different full and partial agonists to assess differential effects of full and partial agonists. This work will be of interest from a fundamental point of view and could provide useful information for the development of new functional ligands.

Materials and methods

Structure preparation

Normal-mode analysis of the PPAR-γ ligand binding domain was done using the X-ray crystal structure of PPAR-γ complexed to rosiglitazone and the coactivator peptide SRC-1 (QTSHKLVQLLTTT) (PDBID: 2PRG) (Nolte et al. 1998). All calculations presented here are of the PPAR-γ LBD monomer. With this crystal structure serving as the initial conformation, calculations of the LDB in the holo state as well as in an apo state, constructed by removing rosiglitazone from chain A of the crystal structure, were done. All calculations were done using the CHARMM program (Brooks et al. 1983) and the all-atom force field for proteins (MacKerell et al. 1998). Prior to hydrogen atom placement, the protonation states of all His residues were determined by macroscopic continuum dielectric calculations (Schaefer and Karplus 1997) using the UHBD program (Madura et al. 1995) and the scripts developed by M. Schaefer (personal communication). All other titratable residues were assigned their standard protonation states at pH 7. The calculations used an internal dielectric constant of 4 and an external dielectric of 80. From the results of these calculations, all histidines were taken to be in the Nε tautomer. The experimental pKa of the thiazolidine-dione in rosiglitazone has a value of 6.8 (Information 1999). Examination of the crystal structure shows that the neighboring Tyr473 residue in the AF-2 domain makes a hydrogen bond to the functional group of the ligand, suggesting that the ligand is deprotonated.

For the thiazolidine-dione ligand, van der Waals parameters were obtained using the QUANTA program (Accelrys). The partial charges were determined from ab initio quantum-mechanics calculation using the Gaussian program (Frisch et al. 1998). After energy-minimizing the unprotonated ligand at the HF/6-31G* basis set level, the ESP charges (Besler et al. 1990) were determined and used directly in all calculations. The final construction of the proton positions was done using the HBUILD facility (Brunger and Karplus 1988) in the CHARMM program.

Unlike molecular dynamics simulations, where results are averaged over many conformations, normal-mode analysis traditionally uses a single, energy-minimized structure. However, this can raise the question of whether the results observed are dependent on that one particular structure. In the present work, we carried out the calculations on ten structures for each binding state, and the results were averaged, thus averaging out small variations due to the use of single structures. Ten different energy-minimized structures were generated following a procedure that began with energy minimization using the steepest-descent method (SD) (Leach 1996). For each SD minimization, a randomly chosen number of steps, up to 9,000, were done. This was followed by up to 30,000 steps of minimization using the adapted basis Newton–Raphson (ABNR) (Leach 1996) algorithm to reach an RMS gradient of 10^{-7} kcal mol^{-1} or less, to ensure that the structure was at the local minimum of the potential energy surface, a necessary condition for the normal-mode analysis. A switching function was used for the van der Waals nonbonded interactions, and a shift function with the distance-dependent dielectric, $\varepsilon = 4r$, was used for the electrostatic interactions. An atom-based 25 Å cutoff was used to include longer-range electrostatic interactions. A normal-mode calculation was carried out for each of the energy-minimized structures.

Normal-mode calculation

Normal-mode analysis has been used to provide insight into collective motions of many different proteins (Delarue and Sanejouand 2002; Gaillard et al. 2007; Ma and Karplus 1998; Mouawad and Perahia 1996; Nam et al. 2006; Tama et al. 2003; Thomas et al. 1996). The theory underlying normal-mode calculations has been presented elsewhere (Brooks et al. 1995; Levitt et al. 1985). The normal-mode analysis was done using the VIBRAN module of the CHARMM program (Brooks et al. 1983). The treatment of the nonbond interactions in the normal-mode calculations was the same as that used for the energy minimization. It was shown in previous studies that the low-frequency modes contribute significantly to large-scale displacements and can provide important information on domain motions (Hayward 2001). Thus, only the first 3,000 lowest-frequency modes were calculated. Test calculations made on

PPAR-γ showed that the properties examined in this work converge within the first 1,500 modes (data not shown); however, the number of modes calculated was doubled to ensure good convergence in all calculations.

Acknowledgments The authors acknowledge financial and computational support from the Université de Strasbourg, the Centre National de la Recherche Scientifique (CNRS), Institut National de la Santé et de la Recherche Médicale (INSERM), the Ministère de la Recherche, the Institut du Développement et des Ressources en Informatique Scientifique (IDRIS), and the Centre Informatique National de l'Enseignement Supérieur (CINES). The authors would like to thank Dr. Isabelle Billas and Dr. Andrew Atkinson for their careful reading of the manuscript.

References

Accelrys The QUANTA program, San Diego, CA, USA

Agarwal AK, Garg A (2002) A novel heterozygous mutation in peroxisome proliferator-activated receptor-gamma gene in a patient with familial partial lipodystrophy. J Clin Endocrinol Metab 87:408–411

Berman HM, Westbrook J, Feng Z, Gilliland G, Bhat TN, Weissig H, Shindyalov IN, Bourne PE (2000) The protein data bank. Nucleic Acids Res 28:235–242

Bernstein FC, Koetzle TF, Williams GJ, Meyer EF Jr, Brice MD, Rodgers JR, Kennard O, Shimanouchi T, Tasumi M (1977) The Protein Data Bank: a computer-based archival file for macromolecular structures. J Mol Biol 112:535–542

Besler BH, Merz KM, Kollman PA (1990) Atomic charges derived from semiempirical methods. J Comput Chem 11:431–439

Brelivet Y, Kammerer S, Rochel N, Poch O, Moras D (2004) Signature of the oligomeric behaviour of nuclear receptors at the sequence and structural level. EMBO Rep 5:423–429

Brooks BR, Bruccoleri RE, Olafson BD, States DJ, Swaminathan S, Karplus M (1983) CHARMM: a program for macromolecular energy minimization and dynamics calculations. J Comp Chem 4:187–217

Brooks BR, Janezic D, Karplus M (1995) Harmonic analysis of large systems. I. Methodology. J Comp Chem 16:1522–1542

Brunger AT, Karplus M (1988) Polar hydrogen positions in proteins: empirical energy placement and neutron diffraction comparison. Proteins Struct Funct Gen 4:148–156

Bruning JB, Chalmers MJ, Prasad S, Busby SA, Kamenecka TM, He Y, Nettles KW, Griffin PR (2007) Partial agonists activate PPARgamma using a helix 12 independent mechanism. Structure 15:1258–1271

Chandra V, Huang P, Hamuro Y, Raghuram S, Wang Y, Burris TP, Rastinejad F (2008) Structure of the intact PPAR-gamma-RXR-alpha nuclear receptor complex on DNA. Nature 350–356

Cooper A, Dryden DT (1984) Allostery without conformational change. A plausible model. Eur Biophys J 11:103–109

Cronet P, Petersen JF, Folmer R, Blomberg N, Sjoblom K, Karlsson U, Lindstedt EL, Bamberg K (2001) Structure of the PPARalpha and -gamma ligand binding domain in complex with AZ 242; ligand selectivity and agonist activation in the PPAR family. Structure 9:699–706

Delarue M, Sanejouand YH (2002) Simplified normal mode analysis of conformational transitions in DNA-dependent polymerases: the elastic network model. J Mol Biol 320:1011–1024

Ebdrup S, Pettersson I, Rasmussen HB, Deussen HJ, Frost Jensen A, Mortensen SB, Fleckner J, Pridal L, Nygaard L, Sauerberg P (2003) Synthesis and biological and structural characterization of the dual-acting peroxisome proliferator-activated receptor alpha/gamma agonist ragaglitazar. J Med Chem 46:1306–1317

Einstein M, Akiyama TE, Castriota GA, Wang CF, McKeever B, Mosley RT, Becker JW, Moller DE, Meinke PT, Wood HB, Berger JP (2008) The differential interactions of peroxisome proliferator-activated receptor gamma ligands with Tyr473 is a physical basis for their unique biological activities. Mol Pharmacol 73:62–74

Ferre P (2004) The biology of peroxisome proliferator-activated receptors: relationship with lipid metabolism and insulin sensitivity. Diabetes 53(Suppl 1):S43–S50

Frauenfelder H, Petsko GA, Tsernoglou D (1979) Temperature-dependent X-ray diffraction as a probe of protein structural dynamics. Nature 280:558–563

Frisch MJ, Trucks GW, Schlegel HB, Scuseria GE, Robb MA, Cheeseman JR, Zakrzewski VG, Montgomery JA Jr, Stratmann RE, Burant JC (1998) Gaussian 98, Revision A, 7. Gaussian Inc., Pittsburgh

Gaillard T, Martin E, San Sebastian E, Cossio FP, Lopez X, Dejaegere A, Stote RH (2007) Comparative normal mode analysis of LFA-1 integrin I-domains. J Mol Biol 374:231–249

Gampe RT Jr, Montana VG, Lambert MH, Wisely GB, Milburn MV, Xu HE (2000) Structural basis for autorepression of retinoid X receptor by tetramer formation and the AF-2 helix. Genes Dev 14:2229–2241

Gee AC, Katzenellenbogen JA (2001) Probing conformational changes in the estrogen receptor: evidence for a partially unfolded intermediate facilitating ligand binding and release. Mol Endocrinol 15:421–428

Hamuro Y, Coales SJ, Morrow JA, Molnar KS, Tuske SJ, Southern MR, Griffin PR (2006) Hydrogen/deuterium-exchange (H/D-Ex) of PPARgamma LBD in the presence of various modulators. Protein Sci 15:1883–1892

Hasstedt SJ, Ren QF, Teng K, Elbein SC (2001) Effect of the peroxisome proliferator-activated receptor-gamma 2 pro(12)ala variant on obesity, glucose homeostasis, and blood pressure in members of familial type 2 diabetic kindreds. J Clin Endocrinol Metab 86:536–541

Hayward S (2001) Normal mode analysis of biological molecules. In: Becker OM, Roux B, Watanabe M (eds) Computational biochemistry and biophysics. Marcel-Dekker, New York, pp 153–168

Hegele RA, Cao H, Frankowski C, Mathews ST, Leff T (2002) PPARG F388L, a transactivation-deficient mutant, in familial partial lipodystrophy. Diabetes 51:3586–3590

Information P (1999) Avandia, rosiglitazone maleate. SmithKline Beecham Pharmaceuticals, Philadelphia

Johnson BA, Wilson EM, Li Y, Moller DE, Smith RG, Zhou G (2000) Ligand-induced stabilization of PPARgamma monitored by NMR spectroscopy: implications for nuclear receptor activation. J Mol Biol 298:187–194

Kallenberger BC, Love JD, Chatterjee VK, Schwabe JW (2003) A dynamic mechanism of nuclear receptor activation and its perturbation in a human disease. Nat Struct Biol 10:136–140

Kliewer SA, Sundseth SS, Jones SA, Brown PJ, Wisely GB, Koble CS, Devchand P, Wahli W, Willson TM, Lenhard JM, Lehmann JM (1997) Fatty acids and eicosanoids regulate gene expression through direct interactions with peroxisome proliferator-activated receptors alpha and gamma. Proc Natl Acad Sci USA 94:4318–4323

Kostadinova R, Wahli W, Michalik L (2005) PPARs in diseases: control mechanisms of inflammation. Curr Med Chem 12:2995–3009

Leach AR (1996) Molecular modelling: principles and applications. Harlow, UK

Lehmann JM, Moore LB, Smith-Oliver TA, Wilkison WO, Willson TM, Kliewer SA (1995) An antidiabetic thiazolidinedione is a high affinity ligand for peroxisome proliferator-activated receptor gamma (PPAR gamma). J Biol Chem 270:12953–12956

Levitt M, Sander C, Stern PS (1985) Protein normal-mode dynamics: trypsin inhibitor, crambin, ribonuclease and lysozyme. J Mol Biol 181:423–447

Li Y, Choi M, Suino K, Kovach A, Daugherty J, Kliewer SA, Xu HE (2005) Structural and biochemical basis for selective repression of the orphan nuclear receptor liver receptor homolog 1 by small heterodimer partner. Proc Natl Acad Sci USA 102:9505–9510

Ludtke A, Buettner J, Schmidt HH, Worman HJ (2007) New PPARG mutation leads to lipodystrophy and loss of protein function that is partially restored by a synthetic ligand. J Med Genet 44:e88

Ma J, Karplus M (1998) The allosteric mechanism of the chaperonin GroEL: a dynamic analysis. Proc Natl Acad Sci USA 95:8502–8507

MacKerell ADJ, Bashford D, Bellott M, Dunbrack RLJ, Evanseck JD, Field MJ, Fischer S, Gao J, Guo H, Ha S, Joseph-McCarthy D, Kuchnir L, Kuczera K, Lau FTK, Mattos C, Michnick S, Ngo T, Nguyen DT, Prodhom B, Reiher WEI, Roux B, Schlenkrich M, Smith JC, Stote R, Straub J, Watanabe M, Wiorkiewicz-Kuczera J, Yin D, Karplus M (1998) All-atom empirical potential for molecular modeling and dynamics studies of proteins. J Phys Chem 102:3586–3616

Madura JD, Briggs JM, Wade RC, Davis ME, Luty BA, Ilin A, Antosiewicz J, Gilson MK, Bagheri B, Scott LR, McCammon JA (1995) Electrostatics and diffusion of molecules in solution: simulations with the University of Houston Brownian Dynamics program. Comp Phys Commun 91:57–95

Mangelsdorf DJ, Thummel C, Beato M, Herrlich P, Schutz G, Umesono K, Blumberg B, Kastner P, Mark M, Chambon P, Evans RM (1995) The nuclear receptor superfamily: the second decade. Cell 83:835–839

Marques O, Sanejouand YH (1995) Hinge-bending motion in citrate synthase arising from normal mode calculations. Proteins 23:557–560

Montanari R, Saccoccia F, Scotti E, Crestani M, Godio C, Gilardi F, Loiodice F, Fracchiolla G, Laghezza A, Tortorella P, Lavecchia A, Novellino E, Mazza F, Aschi M, Pochetti G (2008) Crystal structure of the peroxisome proliferator-activated receptor gamma (PPARgamma) ligand binding domain complexed with a novel partial agonist: a new region of the hydrophobic pocket could be exploited for drug design. J Med Chem 51:7768–7776

Mouawad L, Perahia D (1996) Motions in hemoglobin studied by normal mode analysis and energy minimization: evidence for the existence of tertiary T-like, quaternary R-like intermediate structures. J Mol Biol 258:393–410

Nagy L, Schwabe JW (2004) Mechanism of the nuclear receptor molecular switch. Trends Biochem Sci 29:317–324

Nam K, Maiorov V, Feuston B, Kearsley S (2006) Dynamic control of allosteric antagonism of leukocyte function antigen-1 and intercellular adhesion molecule-1 interaction. Proteins 64:376–384

Nettles KW, Sun J, Radek JT, Sheng S, Rodriguez AL, Katzenellenbogen JA, Katzenellenbogen BS, Greene GL (2004) Allosteric control of ligand selectivity between estrogen receptors alpha and beta: implications for other nuclear receptors. Mol Cell 13:317–327

Nolte RT, Wisely GB, Westin S, Cobb JE, Lambert MH, Kurokawa R, Rosenfeld MG, Willson TM, Glass CK, Milburn MV (1998) Ligand binding and co-activator assembly of the peroxisome proliferator- activated receptor-gamma. Nature 395:137–143

Ostberg T, Svensson S, Selen G, Uppenberg J, Thor M, Sundbom M, Sydow-Backman M, Gustavsson AL, Jendeberg L (2004) A new class of peroxisome proliferator-activated receptor agonists with a novel binding epitope shows antidiabetic effects. J Biol Chem 279:41124–41130

Renaud JP, Moras D (2000) Structural studies on nuclear receptors. Cell Mol Life Sci 57:1748–1769

Sauerberg P, Pettersson I, Jeppesen L, Bury PS, Mogensen JP, Wassermann K, Brand CL, Sturis J, Woldike HF, Fleckner J, Andersen AS, Mortensen SB, Svensson LA, Rasmussen HB, Lehmann SV, Polivka Z, Sindelar K, Panajotova V, Ynddal L, Wulff EM (2002) Novel tricyclic-alpha-alkyloxyphenylpropionic acids: dual PPARalpha/gamma agonists with hypolipidemic and antidiabetic activity. J Med Chem 45:789–804

Schaefer MSM, Karplus M (1997) pH-dependence of protein stability: absolute electrostatic free energy differences between conformations. J Phys Chem B 101:1663–1683

Tama F, Valle M, Frank J, Brooks CL 3rd (2003) Dynamic reorganization of the functionally active ribosome explored by normal mode analysis and cryo-electron microscopy. Proc Natl Acad Sci USA 100:9319–9323

Thomas A, Field MJ, Perahia D (1996) Analysis of the low-frequency normal modes of the R state of aspartate transcarbamylase and a comparison with the T state modes. J Mol Biol 261:490–506

Tsai CJ, del Sol A, Nussinov R (2008) Allostery: absence of a change in shape does not imply that allostery is not at play. J Mol Biol 378:1–11

Uppenberg J, Svensson C, Jaki M, Bertilsson G, Jendeberg L, Berkenstam A (1998) Crystal structure of the ligand binding domain of the human nuclear receptor PPARgamma. J Biol Chem 273:31108–31112

Verma S, Szmitko PE (2006) The vascular biology of peroxisome proliferator-activated receptors: modulation of atherosclerosis. Can J Cardiol 22(Suppl B):12B–17B

Xu HE, Lambert MH, Montana VG, Plunket KD, Moore LB, Collins JL, Oplinger JA, Kliewer SA, Gampe RT Jr, McKee DD, Moore JT, Willson TM (2001) Structural determinants of ligand binding selectivity between the peroxisome proliferator-activated receptors. Proc Natl Acad Sci USA 98:13919–13924